sciendo

VOLUME 17, N° 3 2023
Journal of Automation, Mobile Robotics and Intelligent Systems

Parameter Identification of Space Manipulator's Flexible Joint

Submitted: 5th January 2023; accepted: 16th March 2023

Mateusz Wojtunik, Fatina Liliana Basmadji, Grzegorz Granosik, Karol Seweryn

DOI: 10.14313/JAMRIS/3-2023/24

Abstract:
A manipulator mounted on a satellite is often used to perform active debris removal missions. The space manipulator control system needs to take the dynamic model of the satellite-manipulator system into account because of the influence of the manipulator motion on the position and attitude of the satellite. Therefore, precise modeling of the space manipulator dynamics as well as parameter identification are needed to improve the credibility of the simulation tools. In this paper, we presented the identification of the flexible-joint space manipulator model based on dynamic equations of motion. Experiments were performed in an emulated microgravity environment using planar air bearings. The arbitrarily selected joint-space trajectory was performed by the manipulator's control system. The experiments were repeated multiple times in order to analyze the identification method sensitivity. The identification is based on the Simulink SimMechanics model. Thus, the procedure can be used for any space manipulator without the need to obtain analytical relations for dynamic equations each time. Including joint flexibility and spring viscous damping in the dynamic model allowed it to reflect the experimental measurements better than the reference model could. Identified parameters of the flexible joint have values of the same magnitude as corresponding real system parameters.

Keywords: *Orbital robotics, Mathematical modeling, Parameter identification, Flexible-joint space manipulator, Microgravity simulator*

1. Introduction

The increase of space debris in low Earth orbit (LEO) led to the development of ideas for on-orbit servicing (OOS) and active debris removal (ADR) missions [1]. One of the considered methods for active removal of malfunctioning satellites from Earth's orbit is to utilize a robotic manipulator mounted on a servicing satellite. Several OOS and ADR missions have already been proposed, e.g., European Space Agency (ESA) mission e.Deorbit [2]. The contact between the debris and the satellite-manipulator system has a significant influence on the system dynamics. The dynamics characteristics of impact and contact between the target and the manipulator's end-effector are derived in [3]. The stages (approach, grasping, de-orbit) of the debris removal using the space manipulator are discussed in [4]. After the capture of the debris, the mass and inertia of the target have a significant impact on the system dynamics. Thus, proper control for the detumbling of the system must be proposed [5, 6].

One of the advantages of space manipulators is their high Technology Readiness Level (TRL) in comparison to other methods such as space nets or harpoons [7]. However, designing a control system for the manipulator mounted on the satellite is difficult due to the influence of the manipulator's motion on the position and attitude of the servicing satellite. In close proximity to the target object, we encounter one of the following cases: the system is free-floating, the satellite is fully controlled, or the satellite control is used to give nonzero velocity before the manipulator's operations (tangent capture case) [8]. Most commonly, it is assumed that the Attitude and Orbit Control System (AOCS) for the satellite is turned off because the external forces and torques induced by satellite thrusters can cause undesirable changes of position and orientation of the end-effector, which might lead to a collision with the target object. As a consequence of uncontrollable satellites, the system has conserved momentum and angular momentum; thus, it is nonholonomic [9, 10]. Such systems will be referred to as free-floating (the first case mentioned above). Due to the influence of the manipulator motion on the state of the servicing satellite, it is necessary to design dedicated control laws that depend on the system's dynamic parameters [11]. One of the main concepts for control of the free-floating manipulator is the so-called Dynamic Jacobian, which depends on the state of both the manipulator and the satellite as well as on the mass and inertia parameters of the system [12]. In addition, there are multiple control methods proposed for the satellite-manipulator system, e.g., predictive control [13] and impedance control [14].

Since the control system of the space manipulator takes the dynamic model into account, it is extremely important to design a precise mathematical model of the space manipulator's joint. Dynamic effects that occur in the joint have a significant influence on the system's dynamics. Therefore, including them in the mathematical model allows us to improve the credibility of the simulation tool. The most popular aspects considered in modeling the dynamics of the free-floating manipulator are joint flexibility, friction,

link flexibility, gear kinematics, and gear dynamics. The flexibility of the joint has a large impact on the control system's stability because it might generate undesirable oscillations that can lead to worse positioning of the end-effector or even to the instability of the control system [15]. Modeling of the flexible-joint fixed-base space manipulator was presented in [16, 17]. The dynamic model of the flexible-joint and flexible-link free-floating manipulator was derived in [18], while joint friction was additionally included in [19]. The influence of the link and joint flexibility on the vibrations of the manipulator's end-effector is analyzed in [20], while controlled vibration suppression of a flexible-base flexible-joint space manipulator is discussed in [21]. The flexibility effects of the target capture during the debris removal procedure are discussed in [22]. Target grasping maneuvers of a flexible-link space manipulator are discussed in terms of collision avoidance, aerodynamic effects, and gravity gradient in [23]. The utilization of Kane's method in deriving the dynamic model of a flexible-link space manipulator is presented in [24]. The influence of the nonlinear friction joint torque on the flexible space manipulator's control system was analyzed in [25]. The general expressions for the system's total momentum and angular momentum as well as dynamic equations of motion of flexible-joint free-floating manipulators were presented in [26]. The analysis of the impact of gear kinematics on the free-floating manipulator dynamics was discussed in [27].

The fact that the vast majority of control laws designed for free-floating manipulators depend on the system's dynamic parameters exposes the necessity of experimental parameter identification. There are two main approaches for the identification of a space manipulator's parameters. The first of them takes advantage of the linear parametrization of the dynamic equations of motion [28], while the other one is based on equations for the conservation of total angular momentum of the system [29]. However, the former approach usually requires noise-sensitive measurements of the angular acceleration of the satellite as well as manipulator joint accelerations. On the other hand, some parameters have to be known a priori while using the latter approach (angular momentum equations). A novel method that allows for the full identification of a space manipulator's dynamic parameters with the assumption of perfectly rigid joints is presented in [30], while parameter estimation of flexible space manipulators is discussed in [31].

In this paper, we present the identification of the space manipulator's flexible joint parameters based on several experimental results. The mathematical model of the planar free-floating space manipulator with flexible joints and viscous joint damping is presented. One of the main novelties of the paper is that the experiments were performed with the use of a real flexible-joint manipulator operated on the air-bearing microgravity test-bed. The identification procedure is based on optimization techniques used to match the response of the Simulink SimMechanics model of the system with experimental results. The main goal of the identification is to improve the credibility of the designed system model, while obtaining real values of the flexible-joint parameters is only a secondary goal of the presented research.

The paper is organized as follows. The dynamic model of the system is described in Section 2. The air-bearing microgravity test-bed is presented in Section 3 along with the description of performed experiments. The identification results are presented in Section 4 and discussed in Section 5. The paper is briefly summarized in Section 6.

2. Dynamics of Planar Flexible-Joint Space Manipulator

Let us consider a planar manipulator mounted on a free-floating satellite. The manipulator has n rotational flexible joints. The schematic view of the system is presented in Figure 1. A stationary inertial frame of reference is denoted as Π_{ine}. It is fixed in an arbitrarily selected point in the Cartesian space.

The idea for modeling the flexible joint is schematically depicted in Figure 2. The model is based on connecting a motor (rigid part of the joint) and a link with a torsional spring and a damper (flexible part of the joint). In comparison to the reference model (with perfectly rigid joints), three additional parameters

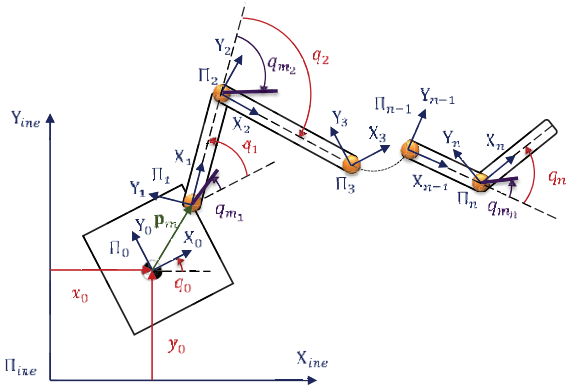

Figure 1. Schematic view of planar n-DoF space manipulator

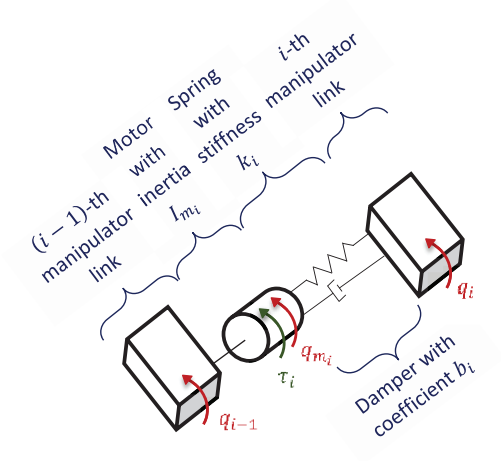

Figure 2. Schematic view of flexible joint with viscous damping

describe the joint: motor inertia, spring stiffness, and viscous damping coefficient.

In order to derive the dynamic equations of motion, we follow the Lagrange formalism. The vector of generalized coordinates for the analyzed planar system is given by:

$$\mathbf{x} = \begin{bmatrix} x_0 & y_0 & q_0 & \mathbf{q}^T & \mathbf{q}_m^T \end{bmatrix}^T \tag{1}$$

where $x_0 \in \mathbb{R}^1$ and $y_0 \in \mathbb{R}^1$ denote the X and Y components of the satellite Center of Mass (CoM) position vector, respectively, $q_0 \in \mathbb{R}^1$ denotes the attitude of the satellite, $\mathbf{q} = \begin{bmatrix} q_1 & \dots & q_n \end{bmatrix}^T \in \mathbb{R}^n$ denotes the vector of manipulator joint angular positions, while $\mathbf{q}_m = \begin{bmatrix} q_{m1} & \dots & q_{mn} \end{bmatrix}^T \in \mathbb{R}^n$ denotes the vector of motor angular positions. It is noteworthy that $\mathbf{q}$ and $\mathbf{q}_m$ are measured with respect to the same frame of reference (see Figure 1).

The second-order Euler-Lagrange equation is given by [32]:

$$\frac{d}{dt}\left(\frac{\partial \mathcal{L}}{\partial \dot{\mathbf{x}}}\right) - \frac{\partial \mathcal{L}}{\partial \mathbf{x}} + \frac{\partial \mathcal{F}}{\partial \dot{\mathbf{x}}} = \mathbf{Q} \tag{2}$$

where $\mathcal{L} \in \mathbb{R}^1$ denotes the Lagrange function of the system, defined as difference between system's total kinetic energy and potential energy, $\mathcal{F} \in \mathbb{R}^1$ denotes Rayleigh's dissipation function, while $\mathbf{Q} \in \mathbb{R}^{3+2n}$ denotes the vector of generalized forces.

In the notation used in (2) we assume that the derivative of a scalar function with respect to a column vector is a column (in order to avoid writing multiple transpositions).

As stated in Section 1, we assume that the servicing satellite is uncontrolled. As a result, the first three entries of the generalized forces vector are equal to zero; thus, $\mathbf{Q} = \begin{bmatrix} 0 & 0 & 0 & \mathbf{0}_{1xn} & \boldsymbol{\tau}^T \end{bmatrix}^T$, where $\mathbf{0}_{1xn} \in \mathbb{R}^n$ denotes vector filled with zeros, while $\boldsymbol{\tau} = \begin{bmatrix} \tau_1 & \dots & \tau_n \end{bmatrix}^T \in \mathbb{R}^n$ denotes the vector of manipulator control torques. It is worth noting that the control torques are applied to the motors (rigid parts of manipulator joints).

In the case of space manipulators, the gravitational potential energy is usually assumed to be equal to zero. In addition, the gravity gradient is neglected due to the relatively small size of the manipulator [33]. Each joint of the manipulator has a potential energy coming from the spring. We assume that the stiffness of the spring is linear [34], which is justified by the fact that the same model was used, e.g., in [16, 17, 26]. Thus, the Lagrange function of the analyzed system is given by:

$$\mathcal{L} = T_0 + T_r + T_m - V \tag{3}$$

Kinetic energies of the satellite $T_0 \in \mathbb{R}^1$, the robotic manipulator $T_r \in \mathbb{R}^1$ and the motors $T_m \in \mathbb{R}^1$ as well as total spring potential energy $V \in \mathbb{R}^1$ are given by:

$$T_0 = \frac{1}{2} m_0 (\dot{x}_0^2 + \dot{y}_0^2) + \frac{1}{2} I_0 \dot{q}_0^2 \tag{4}$$

$$T_r = \sum_{i=1}^{n} \left(\frac{1}{2} m_i |\mathbf{v}_i|^2 + \frac{1}{2} I_i \omega_i^2 \right) \tag{5}$$

$$T_m = \sum_{i=1}^{n} \left(\frac{1}{2} I_{m_i} \omega_{m_i}^2 \right) \tag{6}$$

$$V = \sum_{i=1}^{n} \left(\frac{1}{2} k_i (q_{m_i} - q_i)^2 \right) \tag{7}$$

where $m_0 \in \mathbb{R}^1$ and $I_0 \in \mathbb{R}^1$ denote mass and inertia of the satellite, respectively, $m_i \in \mathbb{R}^1$ and $I_i \in \mathbb{R}^1$ denote mass and inertia of the i-th manipulator link, $\mathbf{v}_i \in \mathbb{R}^2$ denotes the linear velocity of the i-th manipulator link's CoM with respect to Π_{ine}, $|\cdot|$ denotes Euclidean norm, $\omega_i \in \mathbb{R}^1$ denotes the angular velocity of the i-th manipulator link with respect to Π_{ine}, $I_{m_i} \in \mathbb{R}^1$ denotes inertia of the i-th motor, $\omega_{m_i} \in \mathbb{R}^1$ denotes the angular velocity of the i-th motor with respect to Π_{ine}, while $k_i \in \mathbb{R}^1$ is the stiffness of i-th manipulator joint (spring). It is assumed that the mass of each motor is included in the mass of the respective manipulator link; thus, T_m consists only of rotational kinetic energy.

The Rayleigh's dissipation function for the analyzed system is given by:

$$\mathcal{F} = \sum_{i=1}^{n} \left(\frac{1}{2} b_i (\dot{q}_{m_i} - \dot{q}_i)^2 \right) \tag{8}$$

where $b_i \in \mathbb{R}^1$ denotes viscous damping coefficient of the i-th manipulator joint.

After evaluating $\mathbf{v}_i$, ω_i, and ω_{m_i} as functions of generalized coordinates and their derivatives, the Lagrange function and Rayleigh's dissipation function can be directly applied to (2) which yields the dynamic equations of motion of the system:

$$(\mathbf{M}^* + \mathbf{J}^*)\ddot{\mathbf{x}} + (\mathbf{C}^* + \mathbf{B}^*)\dot{\mathbf{x}} + \mathbf{K}^*\mathbf{x} = \mathbf{Q} \tag{9}$$

Relations for matrices that appear in (9) are presented below.

$$\mathbf{M}^* = \begin{bmatrix} \mathbf{M} & \mathbf{0}_{(3+n)xn} \\ \mathbf{0}_{nx(3+n)} & \mathbf{0}_{nxn} \end{bmatrix} \tag{10}$$

$$\mathbf{J}^* = \begin{bmatrix} \mathbf{0}_{2x2} & \mathbf{0}_{2x(1+2n)} \\ \mathbf{0}_{(1+2n)x2} & \mathbf{J} \end{bmatrix} \tag{11}$$

$$\mathbf{C}^* = \begin{bmatrix} \mathbf{C} & \mathbf{0}_{(3+n)xn} \\ \mathbf{0}_{nx(3+n)} & \mathbf{0}_{nxn} \end{bmatrix} \tag{12}$$

$$\mathbf{B}^* = \begin{bmatrix} \mathbf{0}_{3x3} & \mathbf{0}_{3xn} & \mathbf{0}_{3xn} \\ \mathbf{0}_{nx3} & \mathbf{B} & -\mathbf{B} \\ \mathbf{0}_{nx3} & -\mathbf{B} & \mathbf{B} \end{bmatrix} \tag{13}$$

$$\mathbf{K}^* = \begin{bmatrix} \mathbf{0}_{3x3} & \mathbf{0}_{3xn} & \mathbf{0}_{3xn} \\ \mathbf{0}_{nx3} & \mathbf{K} & -\mathbf{K} \\ \mathbf{0}_{nx3} & -\mathbf{K} & \mathbf{K} \end{bmatrix} \tag{14}$$

Matrices $\mathbf{M} \in \mathbb{R}^{(3+n)x(3+n)}$ and $\mathbf{C} \in \mathbb{R}^{(3+n)x(3+n)}$ are mass and Coriolis matrices for the reference model (perfectly rigid manipulator joints), respectively. These matrices depend on satellite and manipulator parameters and explicit relations for them can be found in [35]. Matrices $\mathbf{M}^* \in \mathbb{R}^{(3+2n)x(3+2n)}$ and $\mathbf{C}^* \in$

$\mathbb{R}^{(3+2n)x(3+2n)}$ are filled with zeros, which is a result of expressing motor angular positions with respect to the same frame of reference as flexible joint angular positions.

Matrices $\mathbf{B} \in \mathbb{R}^{nxn}$ and $\mathbf{K} \in \mathbb{R}^{nxn}$ denote damping and stiffness matrices, respectively, given by:

$$\mathbf{K} = \text{diag}(k_1, k_2, \dots, k_n) \tag{15}$$

$$\mathbf{B} = \text{diag}(b_1, b_2, \dots, b_n) \tag{16}$$

where diag denotes an operator that forms a diagonal matrix from given parameters – such a matrix has nonzero components only on its diagonal.

Matrix $\mathbf{J} \in \mathbb{R}^{(1+2n)x(1+2n)}$ is the inertia matrix of manipulator motors given by:

$$\mathbf{J} = \begin{bmatrix} \mathbf{J}_A & \mathbf{0}_{nx1} & \mathbf{J}_B \\ \mathbf{0}_{1xn} & 0 & \mathbf{0}_{1xn} \\ \mathbf{J}_B^T & \mathbf{0}_{nx1} & \mathbf{J}_C \end{bmatrix} \tag{17}$$

where each submatrix is derived as follows:

$$\mathbf{J}_A = \begin{bmatrix} \sum_{i=1}^{n} I_{m_i} & \sum_{i=2}^{n} I_{m_i} & \sum_{i=3}^{n} I_{m_i} & \cdots & \sum_{i=n}^{n} I_{m_i} \\ \sum_{i=2}^{n} I_{m_i} & \sum_{i=2}^{n} I_{m_i} & \sum_{i=3}^{n} I_{m_i} & \cdots & \sum_{i=n}^{n} I_{m_i} \\ \sum_{i=3}^{n} I_{m_i} & \sum_{i=3}^{n} I_{m_i} & \sum_{i=3}^{n} I_{m_i} & \cdots & \sum_{i=n}^{n} I_{m_i} \\ \vdots & \vdots & \vdots & \ddots & \vdots \\ \sum_{i=n}^{n} I_{m_i} & \sum_{i=n}^{n} I_{m_i} & \sum_{i=n}^{n} I_{m_i} & \cdots & \sum_{i=n}^{n} I_{m_i} \end{bmatrix} \tag{18}$$

$$\mathbf{J}_B = \begin{bmatrix} I_{m_1} & I_{m_2} & I_{m_3} & \cdots & I_{m_{n-1}} & I_{m_n} \\ 0 & I_{m_2} & I_{m_3} & \cdots & I_{m_{n-1}} & I_{m_n} \\ 0 & 0 & I_{m_3} & \cdots & I_{m_{n-1}} & I_{m_n} \\ \vdots & \vdots & \vdots & \ddots & \vdots & \vdots \\ 0 & 0 & 0 & \cdots & 0 & I_{m_n} \end{bmatrix} \tag{19}$$

$$\mathbf{J}_C = \text{diag}(I_{m_1}, I_{m_2}, \dots, I_{m_n}) \tag{20}$$

It is noteworthy that the dynamic model considers a slowly rotating motor because gear kinematics are not included. In the real hardware, we expect a quickly rotating motor that is connected with the rigid part of the joint (output shaft) via gearbox. Then, the output shaft is connected with the manipulator link via spring and damper (as seen in Figure 2). Therefore, in order to include inertia of quickly rotating motor in I_{m_i}, its moment of inertia must be multiplied by the square of the gear reduction ratio. In addition, the model presented above can also be used if the manipulator has both rigid and flexible joints. In such situations, the respective sizes of each matrix can vary depending on the number of flexible joints.

3. Description of the Test-Bed and Performed Experiments

We present the identification of flexible joint of the space manipulator based on experiments performed in emulated microgravity environment using dedicated test-bed operated by the Space Research Centre of the Polish Academy of Sciences (CBK PAN) [36, 37].

3.1. Microgravity Air-Bearing Test-Bed

The test-bed consists of a precisely leveled granite table, a planar manipulator mounted on the servicing satellite mock-up, and the operator's computer. The granite table is 3 m x 2 m. Planar air bearings located under both manipulator and satellite mock-ups allow us to emulate microgravity environment via producing a thin film of pressurized air between the surface of the table and air bearings. As a result, the manipulator's motion becomes frictionless in the horizontal plane. The pressurized air is provided by an air tank located on the satellite mock-up. The manipulator has three rotational joints, the first of which is flexible, and the other two are rigid. As a result, $\mathbf{q} = \begin{bmatrix} q_1 & q_2 & q_3 \end{bmatrix}^T$ and $\mathbf{q}_m = q_{m_1}$. The flexibility of the first joint is achieved by introducing the compliant component. CAD models of the flexible joint and the compliant component are presented in Figure 3 [38].

The control system of the manipulator is realized in the joint space and is based on the ATSAMA5D36 microcontroller located on the satellite mock-up. The manipulator joint angular positions are measured via encoders. In addition, an external vision system allows the measurement of position and orientation (with respect to Π_{ine}) of dedicated markers mounted on both the satellite mock-up and the manipulator's end-effector. Each joint has a harmonic gear with a gear reduction ratio of 100 : 1.

Parameters of the manipulator are listed in Table 1. The mass of the satellite mock-up is equal to 58.69 kg,

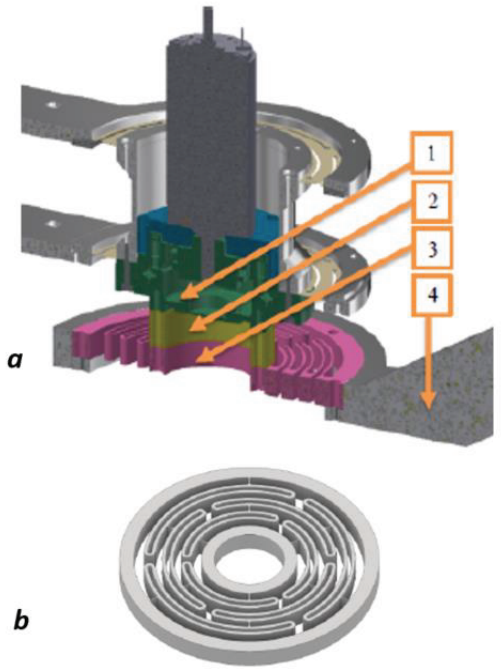

Figure 3. a – CAD model of the flexible joint; b – CAD model of the compliant component; 1 – gear; 2 – sleeve; 3 – compliant component; 4 – connector

Table 1. Parameters of the manipulator

Parameter	Link 1	Link 2	Link 3
Mass [kg]	2.81	2.82	4.64
Moment of inertia [kgm^2]	0.0637	0.0635	0.0515
Length [m]	0.449	0.449	0.310
Position vector of CoM [m]	$\begin{bmatrix}0.1362\\-0.0017\end{bmatrix}$	$\begin{bmatrix}0.1340\\-0.0005\end{bmatrix}$	$\begin{bmatrix}0.1511\\0.0004\end{bmatrix}$

while its moment of inertia is equal to 2.42 kgm^2. The position vector of the manipulator mounting point expressed with respect to Π_0 and rotated to Π_0 is equal to $\mathbf{p}_m^{(\Pi_0)} = \begin{bmatrix}0.337\text{ m} & -0.001\text{ m}\end{bmatrix}^T$. Expressing this vector as rotated to Π_0 is convenient as entries of the vector are then constant.

3.2. Description of the Test Campaign

A set of experiments was performed on the microgravity air-bearing simulator. In each test, the manipulator control system tracks the trajectory defined in the joint space. It is noteworthy that the encoder in the first joint is located before the compliant component. Therefore, the measurements of the encoder relate to the position of the motor q_{m_1} (rigid part of the joint). Hence, in each test the trajectory of the motor angular position will be realized. The discussion concerning obtaining the angular position of the manipulator's flexible joint q_1 will be brought up in the next section.

The initial position and attitude of the satellite are equal to 0 at the beginning of every experiment. Both manipulator and satellite have zero initial velocity. The experiment was repeated 5 times.

The test scenario is chosen arbitrarily. The desired motion of the manipulator is represented by a joint-space trajectory of each joint accelerating with a constant acceleration. The initial condition for the manipulator is: $q_{m_1}(t_0) = 7.5$ deg, $q_2(t_0) = -15$ deg, $q_3(t_0) = -22.5$ deg. The trajectory lasts 10 s.

3.3. Calculation of the Manipulator's Flexible Joint Angular Position

As stated in the previous Section, the encoder in the first joint of the manipulator allows the measurement of the angular position of the motor (rigid part of the joint). In order to obtain the angular position of the flexible joint of the manipulator, the external vision system measurements of the position and attitude of the satellite mock-up and the position and orientation of the end-effector are used. However, it is noteworthy that such measurements will not be available in a real mission on orbit.

In order to obtain the angular position of the flexible joint of the manipulator, we use the direct kinematics equation written for the satellite-manipulator system:

$$\begin{bmatrix}x_e\\y_e\end{bmatrix} = \begin{bmatrix}x_0\\y_0\end{bmatrix} + \mathbf{R}_0\mathbf{p}_m^{(\Pi_0)} + \mathbf{R}_1\begin{bmatrix}l_1\\0\end{bmatrix} + \mathbf{R}_2\begin{bmatrix}l_2\\0\end{bmatrix} + \mathbf{R}_3\begin{bmatrix}l_3\\0\end{bmatrix} \tag{21}$$

where $x_e \in \mathbb{R}^1$ and $y_e \in \mathbb{R}^1$ denote the X and Y components of the end-effector position vector, respectively, $l_i \in \mathbb{R}^1$ denotes the length of the i-th manipulator link, while $\mathbf{R}_0 \in \mathbb{R}^{2x2}$ denotes the rotation matrix of the satellite with respect to Π_{ine}:

$$\mathbf{R}_0 = \begin{bmatrix}\cos(q_0) & -\sin(q_0)\\ \sin(q_0) & \cos(q_0)\end{bmatrix} \tag{22}$$

The variable $\mathbf{R}_i \in \mathbb{R}^{2x2}$ denotes the rotation matrix of the i-th manipulator link with respect to Π_{ine} (with $i = 1, 2, 3$):

$$\mathbf{R}_i = \begin{bmatrix}\cos\left(q_0 + \sum_{j=1}^{i} q_j\right) & -\sin\left(q_0 + \sum_{j=1}^{i} q_j\right)\\ \sin\left(q_0 + \sum_{j=1}^{i} q_j\right) & \cos\left(q_0 + \sum_{j=1}^{i} q_j\right)\end{bmatrix} \tag{23}$$

Equation (21) needs to be solved for q_1 which appears in $\mathbf{R}_1$, $\mathbf{R}_2$ and $\mathbf{R}_3$. Position components of the end-effector x_e, y_e as well as position and attitude of the satellite x_0, x_0, q_0 are measured via external vision system. The angular positions of the second and third joints of the manipulator q_2, q_3 are measured via encoders. For each performed experiment, Equation (21) is used in order to obtain the angular position of the flexible joint of the manipulator.

4. Identification of Flexible Joint Parameters

In order to match the model with the behavior of the manipulator on the air-bearing test-bed, three parameters will be identified: motor inertia I_{m_1}, joint stiffness k_1, and viscous damping coefficient b_1. In addition, it was decided that the initial spring offset $\lambda_1(t_0 = 0) = q_1(t_0 = 0) - q_{m_1}(t_0 = 0)$ will be identified for each experiment. The initial spring offset cannot be controlled on the test-bed. At the beginning of the test, the control system is able to maintain constant angular positions of the motor q_{m_1}, the second joint q_2, and the third joint q_3. However, the angular position of the flexible joint q_1 oscillates around the equilibrium point $q_1 = q_{m_1}$ as a result of spring potential energy. Then, the desired trajectory is loaded to the manipulator's control system, and the spring offset at that current time will lead to different dynamics of the system during trajectory realization. The initial spring offset influences the amplitude of the flexible joint angular position oscillations.

The implemented identification method is based on the optimization technique. The dynamic Equations (9) are linearly parametrized with respect to three above-mentioned flexible joint parameters. Therefore, it is intuitive to use a standard technique such as least-square method with State-Variable Filter (SVF) [39]. However, the initial spring offset appears in the dynamic equations of motion nonlinearly under trigonometric functions. Second, in the case of free-floating manipulators, the analytical derivation of the dynamic equations of motion

is very complicated. Therefore, the goal of the presented work was to implement a procedure that would be based on Simulink SimMechanics model of the system [40]. Designing a Simulink model of the satellite-manipulator system is much easier than deriving analytical relations. The SimMechanics model was validated with the use of analytical expressions for the dynamic model. In the future, the derivation of the dynamic equations of motion will not be needed again, as it is cross-checked that the SimMechanics model gives valid results.

The SimMechanics model can be actuated via two methods: by applying predefined motion of the body or by applying generalized forces. In the presented approach we actuate the motion of the second and third joint of the manipulator with the use of encoder measurements obtained in experiments. The satellite is not actuated in order to comply with the nonholonomic nature of the system. Finally, the motion of the motor (rigid part of the first joint) is actuated with driving torques obtained with the use of inverse dynamics approach for reference (rigid joints) model. The motion of the manipulator's flexible joint is then caused by the dynamic coupling of the spring-damper system. By changing parameters I_{m_1}, k_1, b_1, λ_1 we are able to obtain different motion of the flexible joint.

In order to utilize the SimMechanics model in the identification procedure, we choose the Nelder-Mead method (also called the downhill simplex method) [41]. The cost function for the optimization procedure is chosen as:

$$f_{cost}(\hat{I}_{m_1}, \hat{k}_1, \hat{b}_1, \hat{\lambda}_1) = \sum_{i=1}^{p}((q_{1_{mod}}(t_i, \hat{I}_{m_1}, \hat{k}_1, \hat{b}_1, \hat{\lambda}_1) - q_{1_{ex}}(t_i))^2) \tag{24}$$

where ^ denotes estimation value used in each iteration of the optimization procedure, subscript mod refers to SimMechanics model response, subscript ex refers to the performed experiment (see Section 3.3), while p denotes number of measurements.

The minimum of the cost function means that for the chosen parameters we obtained the best matching between the model response and the experimental results. The identification procedure changes the identified parameters and solves the SimMechanics model in each iteration in order to find the best solution. The lower and upper bounds for each parameter are:

$$0.001\ \text{kgm}^2 < \hat{I}_{m_1} < 100\ \text{kgm}^2$$

$$0.01\frac{\text{Nm}}{\text{rad}} < \hat{k}_1 < 100\frac{\text{Nm}}{\text{rad}}$$

$$0 < \hat{b}_1 < 10\frac{\text{kgm}}{\text{s}}$$

$$-0.1\ \text{rad} < \hat{\lambda}_1 < 0.1\ \text{rad}$$

The identification procedure was performed for each experiment. The angular position of the manipulator's flexible joint for the experiment as well as the simulation of the reference model and the flexible-joint model with identified parameters are presented in Figures 4–8 for each experiment, respectively. The measurements from the vision system and from the encoders contain noise [37]. Therefore, the identified values are rounded to one decimal place so that the identification accuracy is adequate to measurement uncertainty. The obtained values of the flexible joint parameters are listed in Table 2. The identified initial spring offset for each experiment are presented in Table 3. The frames obtained from the vision system during one of the tests are presented in Figure 9.

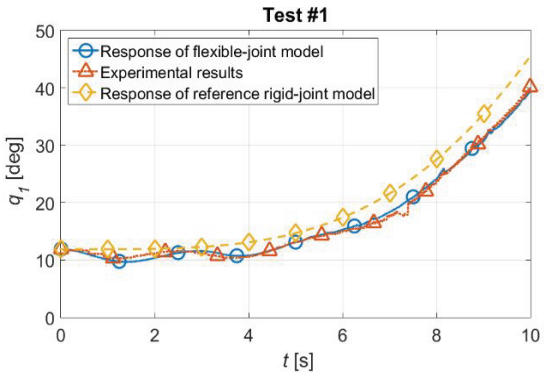

Figure 4. Flexible joint angular position – comparison between model and experimental results for test #1

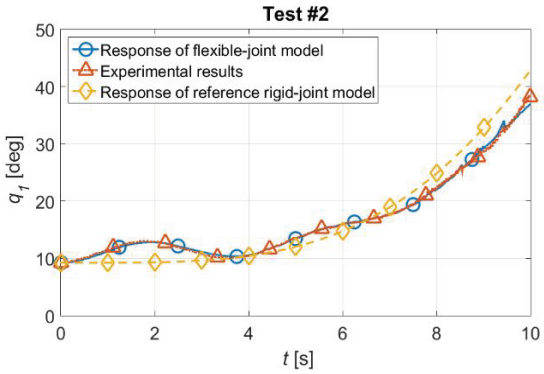

Figure 5. Flexible joint angular position – comparison between model and experimental results for test #2

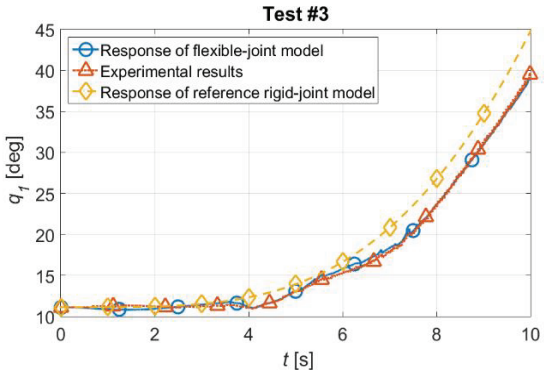

Figure 6. Flexible joint angular position – comparison between model and experimental results for test #3

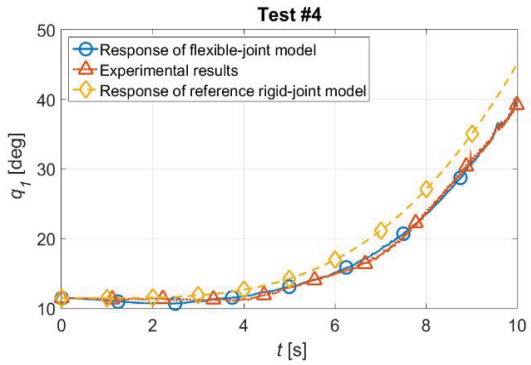

Figure 7. Flexible joint angular position – comparison between model and experimental results for test #4

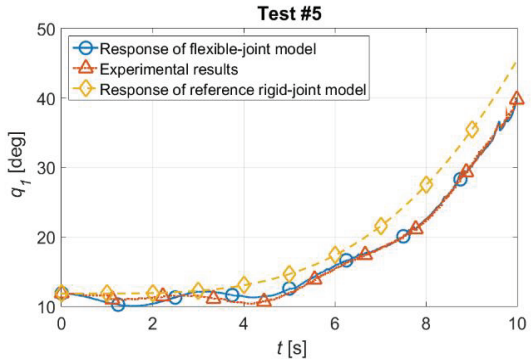

Figure 8. Flexible joint angular position – comparison between model and experimental results for test #5

Table 2. Flexible joint parameter identification results

	Parameter	Motor inertia	Joint stiffness	Damping coefficient
	Symbol	I_{m_1}	k_1	b_1
	Unit	[kgm^2]	$\left[\frac{\text{Nm}}{\text{rad}}\right]$	$\left[\frac{\text{kgm}}{\text{s}}\right]$
Value	Test #1	6.9	12.8	1.3
	Test #2	3.3	5.1	0.4
	Test #3	5.6	9.2	0.5
	Test #4	7.6	5.1	0.0
	Test #5	4.5	8.3	0.1
	Average	5.6	8.1	0.5
	Standard deviation	1.8	3.2	0.5

Table 3. Values of the identified initial spring offset

	Symbol	λ_1
	Unit	[deg]
Value	Test #1	−1.3
	Test #2	2.8
	Test #3	−0.2
	Test #4	−0.4
	Test #5	−1.1

5. Discussion

The identification procedure gave satisfactory results. By analyzing each figure, it can be concluded that in each case the flexible-joint model response reflects the experimental results better than the reference model response. The best matching between the test results and SimMechanics results was obtained for Test #2 (see Figure 5). The frequency and amplitude of oscillations caused by the flexibility of the joint is well illustrated. In other experiments, it is observed that the oscillations caused by the joint flexibility are not as significant. This might be caused by lower initial spring offset which will be discussed in detail below. In addition, it is observed that the motion of the flexible joint in the latter part of the test is more similar to the experimental results for each case of the flexible-joint model simulation.

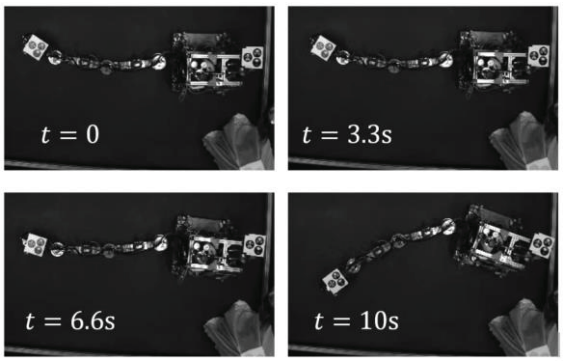

Figure 9. Frames captured by the vision system camera during Test #2

The numerical results for the motor inertia range from 3.3 kgm^2 in Test #2 to 7.6 kgm^2 in Test #4. The average obtained value in the identification is equal to 5.6 kgm^2 $\pm$ 1.8 kgm^2. Although the standard deviation is quite high, the identified values had the same order of magnitude in each case. As explained in Section 2, the motor inertia I_{m_1} in the analyzed model is expected to be very high (identified parameter is one order of magnitude higher than each manipulator link's inertia) because the inertia of the quickly rotating motor must be scaled with the square value of the harmonic gear reduction ratio. The motor inertia influences two main aspects in the model response. First, high I_{m_1} values cause the amplitude of spring oscillations to be greater. Second, this parameter influences the value of the d'Alambert (inertial) reaction forces induced within the system.

The identified value for the joint stiffness is equal to 8.1 $\frac{\text{Nm}}{\text{rad}}$ $\pm$ 3.2 $\frac{\text{Nm}}{\text{rad}}$. The design value of the compliant component can be obtained from the CAD model and is equal to 5.47 $\frac{\text{Nm}}{\text{rad}}$ [38]. This value serves as the only reference despite the fact that the real stiffness of the compliant component might be slightly different than the one obtained using the CAD model. Although the average identified value has the proper order of magnitude, the exact value differs from the design value. However, it is observed that the identification for Test #2 (which was previously concluded to be the best result of all experiments) and Test #4 led to the stiffness value of 5.1 $\frac{\text{Nm}}{\text{rad}}$ which is very similar to the corresponding CAD value. The joint stiffness used in the flexible-joint model allows us to shape the frequency and the amplitude of spring oscillations. For instance, it can be clearly seen in Figure 4 that the

frequency of the oscillations is not identical to that of the experiment. The identified stiffness for this case is very high. However, the latter parts of the simulation response are very close to the experimental results. The procedure may be improved by introducing a scaling factor so that the cost function values the first part of the experiment higher than the latter parts because the flexibility of the joint at the end of the experiment was damped.

It must be here repeated (as previously stated in Section 1) that the main purpose of the identification was to improve the credibility of the simulation tool, not to identify real system parameters. On the other hand, the obtained standard deviation is high, which might lead to a conclusion that the compliant component's stiffness is not linear, and the proposed spring model might be imprecise.

The results for the damping coefficient were unsatisfactory, e.g., the procedure identified no damping for Test #4 and very high damping for Test #1. This leads to a conclusion that the friction of the spring is not linear; hence, the proposed model for the oscillation damping is not correct. Future work might include identification of friction forces induced within both the motor (rigid part of the joint) and compliant component.

Finally, in each experiment, the initial spring offset was different. As explained before, this value cannot be controlled in any way during the tests. In Test #2 (identified as the best example from performed experiments), the highest initial spring offset was equal to 2.8 deg. On the other hand, Figure 6 shows that in Test #3 almost no oscillations at the first part of the test were obtained. The initial spring offset for this test was much lower and equal to −0.2 deg. As a result, the joint stiffness identified for this case is very different than the reference value (CAD model). It is intuitive that the identification procedure is very sensitive to initial spring offset. If the offset is high, we achieve greater excitation of identified parameters, which is very important in parameter identification. Consequently, the results are more credible if the parameter excitation is large enough, and we desire as high initial spring potential energy as possible in order to obtain good identification results.

6. Conclusion

In this paper, we have proposed the space manipulator's flexible joint parameter identification based on experiments performed in an emulated microgravity environment. The experiments were performed using the test-bed based on air bearings. The manipulator has a flexible first joint, which allows testing of the motion of the flexible-joint manipulator and comparison with the simulation results.

The performed identification results are satisfactory, although various problems were observed in the proposed approach. The identified motor inertia seems high, but the results are correct as the value should account for the quickly rotating motor inertia scaled with the square of the gear reduction ratio. The identified joint stiffness value has the same order of magnitude as it was obtained from the CAD model. The quality of the identification highly depends on the initial spring offset – higher offsets achieved better the identifications. High initial offset allows greater excitation of identified parameters, which is very important in parameter identification. Finally, the obtained damping coefficients are very different in each experiment, which leads to a conclusion that the spring friction is nonlinear and the proposed model is inadequate.

Future work might include utilizing the nonlinear friction model in the identification procedure and modification of the test-bed so that the initial spring offset can be controlled.

AUTHORS

Mateusz Wojtunik* – The Space Research Centre of the Polish Academy of Sciences (CBK PAN),ul. Bartycka 18a, 00-716 Warsaw, Poland, e-mail: mwojtunik@cbk.waw.pl.

Fatina Liliana Basmadji – The Space Research Centre of the Polish Academy of Sciences (CBK PAN),ul. Bartycka 18a, 00-716 Warsaw, Poland, e-mail: fbasmadji@cbk.waw.pl.

Grzegorz Granosik – Lodz University of Technology, Institute of Automatic Control, Poland, e-mail: grzegorz.granosik@p.lodz.pl.

Karol Seweryn – The Space Research Centre of the Polish Academy of Sciences (CBK PAN),ul. Bartycka 18a, 00-716 Warsaw, Poland, e-mail: ksewerynn@cbk.waw.pl.

*Corresponding author

ACKNOWLEDGEMENTS

This work was partially supported by the Polish National Centre for Research Development, project no. LIDER/19/0119/L-10/18/NCBR/2019.

The authors would like to thank Dr. Tomasz Rybus from Centrum Badań Kosmicznych Polskiej Akademii Nauk (CBK PAN) for his helpful suggestions.

References

[1] C. Bonnal, J. M. Ruault, and M. C. Desjean. "Active debris removal: Recent progress and current trends," *Acta Astronautica*, vol. 50, 2013, pp. 71–96; doi: 10.1016/j.actaastro.2012.11.009.

[2] S. Estable, et al. "Capturing and deorbiting Envisat with an Airbus Spacetug. Results from the ESA e.deorbit Consolidation Phase study," *Journal of Space Safety Engineering*, vol. 7, no. 1, 2020, pp. 52–66; doi: 10.1016/j.jsse.2020.01.003.

[3] P. Huang, Y. Xu, and B. Liang. "Contact and impact dynamics of space manipulator and free-flying target," *Proceedings of the 2005 IEEE/RSJ International Conference on Intelligent Robots and Systems*, Edmonton, AB, Canada, 2005; doi: 10.1109/IROS.2005.1545260.

[4] L. Felicetti, P. Gasbarri, A. Pisculli, M. Sabatini, and G. B. Palmerini. "Design of robotic manipulators for orbit removal of spent launchers' stages," *Acta Astronautica*, vol. 119, 2016, pp. 118–130; doi: 10.1016/j.actaastro.2015.11.012.

[5] F. Aghili. "Optimal control of a space manipulator for detumbling of a target satellite," *Proceedings of the 2009 IEEE International Conference on Robotics and Automation*, Kobe, Japan, 2009; doi: 10.1109/ROBOT.2009.5152235.

[6] B. Zhan, M. Jin, G. Yang, and C. Zhang. "A novel strategy for space manipulator detumbling a non-cooperative target with collision avoidance," *Advances in Space Research*, vol. 66(4), 2020, pp. 785–799; doi: 10.1016/j.asr.2020.05.045.

[7] M. Shan, J. Guo, and E. Gill. "Review and comparison of active space debris capturing and removal," *Progress in Aerospace Sciences*, vol. 80, 2016, pp. 18–32; doi: 10.1016/j.paerosci.2015.11.001.

[8] K. Seweryn, F. L. Basmadji, and T. Rybus. "Space robot performance during tangent capture of an uncontrolled target satellite," *The Journal of the Astronautical Sciences*, vol. 69, 2022, pp. 1017–1047; doi: 10.1007/s40295-022-00330-2.

[9] I. Dulêba. "Impact of control representations on efficiency of local nonholonomic motion planning," *Biuletyn of the Polish Academy of Sciences Technical Sciences*, vol. 59, no. 2, 2011, pp. 213–218; doi: 10.2478/v10175-011-0026-x.

[10] J. Ratajczak, and K. Tchoń. "Normal forms and singularities of non–holonomic robotic systems: a study of free–floating space robots," *Systems & Control Letters*, vol. 138, 2020, 104661; doi: 10.1016/j.sysconle.2020.104661.

[11] A. Ellery. "Tutorial Review on Space Manipulators for Space Debris Mitigation," *Robotica*, vol. 8, no. 2, 2019; doi: 10.3390/robotics8020034.

[12] K. Yoshida, and Y. Umetani. "Control of a space free–flying robot," *Proceedings of the 29^{th} IEEE Conference on Decision and Control*, Honolulu, USA, 1990; doi: 10.1109/CDC.1990.203553.

[13] T. Rybus, K. Seweryn, and J. Z. Sąsiadek. "Application of predictive control for manipulator mounted on a satellite," *Archives of Control Sciences*, vol. 28, no. 1, 2018, pp. 105–118; doi: 10.24425/119079.

[14] P. Palma, K. Seweryn, and T. Rybus. "Impedance control using selected compliant prismatic joint in a free-floating space manipulator," *Aerospace*, vol. 9, no. 8, 2022, p. 406; doi: 10.3390/aerospace9080406.

[15] J. Z. Sąsiadek. "Space robotics and its challenges," *Aerospace Robotics*, Springer, 2013, pp. 1–8; doi: 10.1007/978-3-642-34020-8_1.

[16] J. Qingxuan, Z. Xiaodong, S. Hanxu, and C. Ming. "Active control of space flexible–joint/flexible–link manipulator," *Proceedings of the 2008 IEEE Conference on Robotics, Automation and Mechatronics*, Chengdu, China, 2008, pp. 812–818; doi: 10.1109/RAMECH.2008.4681344.

[17] S, Ulrich, J. Z. Sąsiadek, and I. Barkana. "Modeling and direct adaptive control of a flexible–joint manipulator," *Journal of Guidance, Control, And Dynamics*, vol. 35, no. 1, 2012, pp. 25–39; doi: 10.2514/1.54083.

[18] X.-Y. Yu. "Augmented robust control of a free–floating flexible space robot," *Journal of Aerospace Engineering*, vol. 229, no. 5, 2015, pp. 947–957; doi: 10.1177/0954410014541632.

[19] D. Meng, Y. She, W. Xu, W. Lu, and B. Liang. "Dynamic modeling and vibration characteristics analysis of flexible-link and flexible-joint space manipulator," *Multibody System Dynamics*, vol. 43, 2018, pp. 321–347; doi: 10.1007/s11044-017-9611-6.

[20] X. Liu, H. Li, J. Wang, and G. Cai. "Dynamics analysis of flexible space robot with joint friction," *Aerospace Science and Technology*, vol. 47, 2015, pp. 164–176; doi: 10.1016/j.ast.2015.09.030.

[21] Z. Chen, Y. Zhang, and Z. Li. "Hybrid Control Scheme Consisting of Adaptive and Optimal Controllers for Flexible-Base Flexible-Joint Space Manipulator with Uncertain Parameters," *Proceedings of the 2017 9th International Conference on Intelligent Human-Machine Systems and Cybernetics* (IHMSC), Hangzhou, China, 2017; doi: 10.1109/IHMSC.2017.84.

[22] A. Stolfi, P. Gasbarri, and M. Sabatini. "A parametric analysis of a controlled deployable space manipulator for capturing a non-cooperative flexible satellite," *Acta Astronautica*, vol. 148, 2018, pp. 317–326; doi: 10.1016/j.actaastro.2018.04.028.

[23] C. Toglia, M. Sabatini, P. Gasbarri, and G. B. Palmerini. "Optimal target grasping of a flexible space manipulator for a class of objectives," *Acta Astronautica*, vol. 68(7-8), 2011, pp. 1031–1041; doi: 10.1016/j.actaastro.2010.09.013.

[24] R. Masoudi, and M. Mahzoon. "Maneuvering and Vibrations Control of a Free-Floating Space Robot with Flexible Arms," *Journal of Dynamic Systems, Measurement and Control*, vol. 133(5), 2011, 051001; doi: 10.1115/1.4004042.

[25] D. Shang, X. Li, M. Yin, and F. Li. "Tracking control strategy for space flexible manipulator considering nonlinear friction torque based on adaptive fuzzy compensation sliding mode controller," *Advances in Space Research*, In Press, 2020; doi: 10.1016/j.asr.2022.04.042.

[26] K. Nanos, and E. Papadopoulos. "On the dynamics and control of flexible joint space manipulator," *Control Engineering Practice*, vol. 45, 2015, pp. 230–243; doi: 10.1016/j.conengprac.2015.06.009.

[27] M. Wojtunik, and K. Seweryn. "The influence of the gear reduction ratio on the free–floating space manipulator's dynamics," *Proceedings of the 18th International Conference on Informatics in Control, Automation and Robotics* (ICINCO 2021), 2021, pp. 282–289; doi: 10.5220/0010556502820289.

[28] H. Wang, and Y. Xie. "Prediction error based adaptive Jacobian tracking for free–floating space manipulators," *IEEE Transactions on Aerospace and Electronic Systems*, vol. 48, no. 4, 2012, pp. 3207–3221; doi: 10.1109/TAES.2012.6324694.

[29] O. Ma, H. Dang, and K. Pham. "On–orbit identification of inertia properties of spacecraft using a robotic arm," *Journal of Guidance, Control, and Dynamics*, vol. 31, no. 6, 2008, pp. 1761–1771; doi: 10.2514/1.35188.

[30] O.-O. Christidi-Loumpasefski, C. Ntinos, and E. Papadopoulos. "Analytical and experimental parameter estimation for free–floating space manipulator systems," *Proceedings of the 14th Symposium on Advanced Space Technologies in Robotics and Automation* (ASTRA '17), Leiden, The Netherlands, 2017.

[31] O.-O. Christidi-Loumpasefski, C. Ntinos, and E. Papadopoulos. "On parameter estimation of flexible space manipulator systems," *Proceedings of the 2020 IEEE/RSJ International Conference on Intelligent Robots and Systems* (IROS), Las Vegas, NV, USA, 2020; doi: 10.1109/IROS45743.2020.9340768.

[32] Goldstein H., Poole C., and Safko J., *Classical Mechanics*, Third Edition, Pearson: London, 2001.

[33] F. Cavenago, A. M. Giordano, and M. Massari. "Contact force observer for space robots," *Proceedings of the 58th Conference on Decision and Control*, Nice, France, 2019; doi: 10.1109/CDC40024.2019.9029285.

[34] Schaub H., and Junkins J. L., *Analytical mechanics of aerospace systems*, AIAA: Reston, VA, 2002.

[35] T. Rybus, M. Wojtunik, and F. L. Basmadji. "Optimal collision-free path planning of a free-floating space robot using spline-based trajectories," *Acta Astronautica*, vol. 190, 2022, pp. 395–408; doi: 10.1016/j.actaastro.2021.10.012.

[36] J. Oleś, J. Kindracki, T. Rybus, Ł. Mężyk, P. Paszkiewicz, R. Moczydłowski, T. Barciński, K. Seweryn, and P. Wolański. "A 2D microgravity test-bed for the validation of space robot control algorithms," *Journal of Automation, Mobile Robotics & Intelligent Systems*, vol. 11, no. 2, 2017, pp. 95–104; doi: 10.14313/JAMRIS_2-2017/21.

[37] F. L. Basmadji, G. Chmaj, T. Rybus, and K. Seweryn. "Microgravity testbed for the development of space robot control systems and the demonstration of orbital maneuvers," *Proceedings of SPIE: Photonics Applications in Astronomy, Communications, Industry and High–Energy Physics Experiments*, Wilga, Poland, 2019; doi: 10.1117/12.2537981.

[38] R. Moczydłowski. "Design of elastic element dedicated for space manipulator joint based on FEM topological optimization," master's thesis (in Polish: "Projekt elementu podatnego pary kinematycznej manipulatora satelitarnego bazuj[1]cy na optymalizacji topologicznej z wykorzystaniem oprogramowania MES"), Warsaw University of Technology, 2017.

[39] Garnier H., and Wang L. *Advances in industrial control: Identification of continuous – time models from sampled data*, Springer, London, 2003.

[40] G. Wood, and D. Kennedy. "Simulating Mechanical Systems in Simulink with SimMechanics," Technical report, The MathWorks, Inc., Natick, USA, 2003.

[41] J. C. Lagarias, J. A. Reeds, M. H. Wright and P. E. Wright. "Convergence properties of the Nelder–Mead simplex method in low dimensions," SIAM Journal of Optimization, vol. 9, no. 1, 1998, pp. 112–147; doi: 10.1137/S1052623496303470.